The Impact of Modern Tobacco Agriculture Planning on the Spatio-temporal Evolution of Urban Construction Land

Miao Yahui, Master
JiangCe, Master
GuZifan, Master
Xi Zenglei, Professor

Miao Yahui, Master of Economics, School of Economics, Hebei University, Baoding, China. Jiang Ce, Master of Economics, School of Economics, Hebei University, Baoding, China. GuZifan, Master of Economics, School of Economics, Hebei University, Baoding, China. Xi Zenglei, Professor of Economics, School of Economics, Hebei University. Research Center or Resources Utilization and Environmental Conservation, Hebei University, Baoding, China. Correspondence author: Xi Zenglei, hbuxzl@hbu.edu.cn

Abstract: In recent years, the world tobacco industry has shown a trend of continuous growth in market demand and increasingly concentrated tobacco market, which brings new opportunities to the tobacco agriculture development. However, the modern tobacco agriculture is bound to occupy a large amount of agricultural land, which will have a certain impact on the distribution of urban construction land (UCL). Therefore, reasonable and effective modern tobacco agricultural planning plays a vital role in promoting modern agricultural and urban development.In this paper, we took Baiyangdian basin as the study area, applying the long time series nighttime light (NTL) data to extract UCL and analysing the impact of modern tobacco agriculture planning on the spatio-temporal evolution of UCL. Firstly, we used a power function model to fit the two kinds of international mainstream NTL data to form a long time series NTL dataset from 1992 to 2018 to make the NTL data comparable over a long time. Then, the threshold segmentation method based on land use data calibration was applied to extract the UCL in Baiyangdian basin in 2000, 2010 and 2018, and to analyze its spatio-temporal evolution characteristics and patterns by combining the landscape metrics and gravity model. The results show that the UCL in Baiyangdian basin shows the expansion trend centered on the main urban area of Baoding City, land intensification degree has increased, and the modern tobacco agriculture planning has a profound impact on the spatio-temporal distribution of UCL. Our study will provide technical support and experience for the scientific modern tobacco agriculture planning.

Keywords: moderntobacco agriculture planning; urban construction land; long time series nighttime light dataset; spatio-temporal evolution
Tob Regul Sci.™ 2021;7(5): 938-949
DOI: doi.org/10.18001/TRS.7.5.12

Modern tobacco agriculture is an important part of modern agriculture and an important branch of agricultural modernization. Developing modern tobacco agriculture plays an important role in realizing agricultural modernization and promoting the development of modern agriculture. Modern tobacco agriculture is an extension of modern agriculture. The concept of modern tobacco agriculture is mainly to encourage farmers to implement large-scale planting, realize intensive and information management of tobacco agriculture on the basis of increasing industrial scale, and enhance the output level and value of tobacco agriculture.[1] Of course, if we want to achieve this goal, we should also increase investment in basic agricultural supporting facilities, such as tobacco and water supporting facilities, and unified education supporting facilities, so as to lay a solid foundation for the modernization of tobacco agriculture. In addition, vigorously developing the experimental field of tobacco agriculture, expanding the cultivation of new varieties, expanding the planting area of tobacco and adjusting the industrial structure of tobacco planting are also the development conditions for realizing the specialization of tobacco agriculture. This change is not only the change of tobacco planting methods and patterns, but also the scientific development mode of the whole process of tobacco planting guided by the advanced concepts of modern production management. The focus of all the above work is to firmly grasp the actual essence of increasing the yield per unit area, improving the quality, increasing the income of tobacco farmers and meeting the needs of industrial enterprises, further improve the organizational form of tobacco production, increase the policy research on agriculture, especially tobacco agriculture protection, and increase the combination of theory and practice, so as to provide reliable guarantee for the development of modern tobacco agriculture.

Modern tobacco agriculture has the following characteristics: First, the production mode of tobacco leaves has been modernized. The whole production process of tobacco leaves, from cultivation to management of tobacco leaves at seedling stage, to baking and preservation of tobacco leaves, has basically achieved mechanization, which not only improves the production efficiency of land, but also greatly reduces the hardship of farmers. Secondly, the management of tobacco cultivated land has been modernized. Mechanized and modern production environment not only improves the tobacco production efficiency, but also improves the tobacco production environment, greatly reduces the environmental pollution caused by the traditional agricultural production process and improves the environmental quality. Thirdly, science and technology play a major role in agricultural production. In the process of tobacco production, new technologies have played an indelible role from the cultivation of tobacco varieties, to the management of new technologies to the later sales information management. Fourthly, the management means should be modernized. Through modern management, the planting area is appropriately increased, the modern level of tobacco production is improved, and the management means are more scientific. Fifthly, the market is more targeted. Market has become the target of tobacco production. Production management began to develop towards enterprise and brand. Sixth, the protection for farmers has been improved. This can greatly reduce farmers' losses when natural disasters and market risks occur. Finally, the scientific quality of farmers has been greatly improved. With the increase of scientific and technological training for farmers, farmers can receive new technologies more efficiently and have a more flexible vision.[2]Because of these, scientific and rational modern tobacco agriculture planning will have a positive and effective impact on the development of agricultural modernization, and will also guide the rational development of urban planning and construction to a certain extent.

Due to the development and popularization of remote sensing technology, more and more scholars realize that the traditional land use monitoring methods can no longer adapt to the ever-changing land use changes, which makes satellite remote sensing earth observation technology the most widely used and effective information technology for monitoring land use changes.[3] Among them, the nighttime light (NTL) imagery is one of the most popular data sources to extract information about urban construction land (UCL), which mainly uses Defense Meteorological Satellite Program/Operational Linescan System (DMSP/OLS) and National Polar-Orbiting Partnership/Visible Infrared Imaging Radiometer Suite (NPP/VIIRS) data. After Croft (1978) first described the feasibility of using DMSP/OLS to extract UCL,[4] many scholars carried out in-depth research on the extraction of UCL, urban scope and extraction algorithm from NTL data.[5,6] According to the literature review, it is found that the UCL extraction based on single NTL data source mainly uses the threshold method, including five research methods: the best threshold estimation method based on clustering analysis,[7] mutation detection method,[8] threshold segmentation method based on brightness gradient,[9] adaptive threshold extraction method[10,11] and reference comparison method.[12] The data sources of the first four methods are relatively single, which cannot avoid the problems of fuzzy and inaccurate extraction boundary caused by lack of reference and comparison. Hence, the reference comparison method is applied in this study, including statistical data reference and remote sensing imagery reference. Statistical data reference method can extract the UCL by selecting the threshold closest to the UCL area published by official statistics as the optimal threshold,[13] and the remote sensing imagery reference method defines the urban area by processing remote sensing imagery like land use imagery, which is used as auxiliary data to complete the extraction of UCL combined with NTL data.[14]

Under the rapid development of urbanization, the land use pattern has become the most direct expression of urbanization, and the expansion of urban land is mainly reflected in the expansion of the scale of UCL. In pace with the development of various remote sensing data especially medium and high resolution land use data, more and more scholars have applied it to the extraction of UCL, and mainly take advantage of methods such as basin algorithm,[15] statistical-vegetation index method,[16] the normalized difference vegetation index (NDVI) modified threshold extraction method[17] and so on. The combination of NTL data and other remote sensing data makes the research result more accurate and more objective owing to these can be compared and verified with each other.

Although the diversification of data sources improves the extraction accuracy of UCL, the extraction of UCL in specific years does not reflect its long time changes. For example, if the research with a long time span is involved, there will be a situation that the sources of NTL data cannot be unified, and because of the lack of comparable basis among the data, the extraction accuracy cannot be discussed. In addition, most of the existing studies are based on national, provincial, municipal, county, city cluster, economic zone and other administrative regional scales, while studies involving natural geographic scales such as basins are still in the exploration stage. Thus, our study proposed a new solution to the above problems by fitting a series of modified NPP/VIIRS data for long time comparison analysis based on DMSP/OLS to build a long time series NTL dataset from 1992 to 2018. Furthermore, our study overcomes the drawback of unverifiability of a single data source and adopts the multi-source data including NTL data, land use data and statistical data, which not only avoids the subjectivity of traditional statistical data, but ensures that these data can be mutually verified and complementary, and takes Baiyangdian basin as the empirical study area to extract UCL and analyze its spatio-temporal evolution impacted by modern tobacco agriculture planning to provide technical support and decision-making reference for the modern tobacco agriculture planning and high-quality economic and ecological development.

STUDY AREA AND DATA

Study area

Baiyangdian basin is the catchment area of the Tang River, the Juma River, the Fu River and other river systems, located between 113°39′E to 116°13′E, 38°9′N to 40°3′N, from T'ai-hang Mountains in the west to North China Plain in the east, with a total basin area of 31,816.46 km² and the basin boundary is 1,008.88 km.[18] It contains 48 counties (or districts) of 11 prefecture-level cities in Baoding, Shijiazhuang, Cangzhou, Zhangjiakou, Hengshui, Langfang in Hebei Province, Datong and Xinzhou in Shanxi Province, Fangshan District, Fengtai District and Mentougou District in Beijing, most of which are located in the administrative division of Baoding City. Baiyangdian basin is the core waters and direct reflection of resource and environmental carrying capacity of the Xiong'an New Area, as well as an important ecological support for the Beijing-Tianjin-Hebei synergistic development and the high quality of the Beijing-Tianjin-Hebei world-UCLass urban agglomeration, which has a prominent strategic position in China’s regional economic development pattern in the new era. The administrative division of Baiyangdian basin based on Landsat 8 remote sensing imagery is shown in Figure 1.

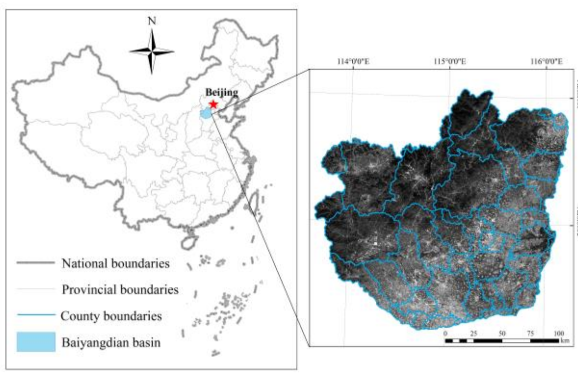

Figure. 1 Administrative division map of Baiyangdian basin in 2018 based on Landsat 8 remote sensing imagery

.

Study data

Data source

DMSP/OLS NTL imagery

The DMSP/OLS NTL data for the study is obtained from National Oceanic and Atmospheric Administration’s (NOAA’s) National Centers for Environmental Information (https://www.ngdc.noaa.gov/eog/dmsp/downloadV4composites.html) for 2000 and 2010. It is displayed by gray value, and the data applied in this study are all from the annual product version of stable NTL data because it has removed the influence of noise such as firelight and cloud, and then obtained by averaging monthly products. Its grid resolution is 1km×1km, and digital number (DN) value is 1 to 63, and the larger the value, the stronger the brightness of NTL and the closer it is to the central area of the city. DMSP/OLS data will be discontinuous and incomparable due to different sensors, different systems and different regional environments in different time periods. Thereby, it is necessary to make mutual calibration, saturation calibration, year-by-year calibration and continuity calibration between sensors before extracting and analyzing the distribution of UCL by using DMSP/OLS data.

NPP/VIIRS NTL imagery

NPP/VIIRS NTL imagery is gained from Colorado School of Mines (https://eogdata.mines.edu/download_dnb_composites.html), and it has better performance than DMSP/OLS data in terms of spatial resolution, temporal resolution and radiometric resolution, and can effectively make up for the shortcoming that the latter cannot detect the weak lights in urban areas in the basin. The spatial resolution of this data is 500m×500m, and it is divided into monthly and annual products. The data used for this study is the monthly average NTL data excluding stray light but retaining the influence of fire light, cloud light and other lights. The time range is from April 2012 to December 2018, with a total of 81 images. As NPP/VIIRS data itself is not saturated, it is better than DMSP/OLS data in the analysis of urban problems.

Land use imagery

In this paper, three periods of Chinese land use remote sensing monitoring images in 2000, 2010 and 2018 provided by Resources and Environment Science and Data Center, Chinese Academy of Sciences (https://www.resdc.cn/) are used as the auxiliary data for UCL extraction. These images are based on Landsat series remote sensing images of American land satellite, and obtained by many professional geographic research institutions through manual visual interpretation and field investigation. Their spatial resolution is 30m×30m, and their production process is scientific, rigorous, objective and accurate. Consequently, they are used as prior auxiliary data to determine the best segmentation threshold for extracting the scope of UCL.

Data processing

The DMSP/OLS calibrated dataset from 1992 to 2013 was obtained by using the invariant target region calibration method to achieve inter-calibration between sensors, saturation calibration, year-by-year calibration and continuity calibration of original DMSP/OLS data. The NPP/VIIRS data was pre-processed with noise reduction and upper limits, and the original DMSP/OLS data in 2013 was used as a reference to fit the NPP/VIIRS data to create a long time NTL series dataset.

DMSP/OLS data calibration

(1) Inter-calibration between sensors

In this study, the invariant target region method was adopted, that was, a constant target area was selected as a reference to correct the nationwide NTL data, and the calibrated DMSP/OLS dataset was established. Since the socio-economic development of Hegang City, Heilongjiang Province, was maintained at a stable level with small changes in urban dynamics, low degree of variation in light values, and high correlation of light values between different sensors during the study period,[19] it was chosen as the invariant target region, and the F16_20051128-20061224 radiometric calibration NTL data was utilized to calibrate the nationwide 34 periods of NTL images under different sensors. Firstly, the DMSP/OLS data was resampled to adjust its spatial resolution to 1km×1km, and secondly, this data was reprojected to Gauss-Kruger projection with a central longitude of 117°. The raster operation in ArcGIS 10.2 software was performed to determine the regression coefficients by using the image self-calibration method with the DN values in the F16_2006 radiometric calibration data as the dependent variable and those of a total of 34 periods of data as the independent variables for curve estimation. After several regression experiments, the power function model with the highest goodness of fit was selected to calibrate the DMSP/OLS data from different sensors according to the following power function model, as shown in equation (1):

$$\mathrm{DN_F} = a \times \mathrm{DN}^b \tag{1}$$

where $\mathrm{DN_F}$ represents the gray value after calibration, DN represents the gray value before calibration, a and b are the parameters after regression, respectively, and the regression parameters are shown in Table 1. By considering the study period as well as the goodness of fit, it was decided to select the calibrated data of F14_2000 and F18_2010 as the study data of 2000 and 2018, respectively.

Table 1 Inter-calibration parameters between DMSP/OLS sensors

Sensors	R^2	*p*-value	*a*	*b*
F101992	0.615	0.000	2.411	0.841
F101993	0.770	0.000	0.984	1.235
F101994	0.753	0.000	1.308	1.111
F121994	0.611	0.000	3.239	0.748
F121995	0.792	0.000	1.211	1.100
F121996	0.767	0.000	1.610	0.999

F121997	0.767	0.000	1.091	1.132
F121998	0.819	0.000	0.838	1.186
F121999	0.724	0.000	1.218	1.072
F141997	0.744	0.000	2.516	0.923
F141998	0.772	0.000	1.208	1.156
F141999	0.800	0.000	1.439	1.132
F142000	0.841	0.000	1.221	1.123
F142001	0.854	0.000	1.174	1.125
F142002	0.789	0.000	1.640	0.977
F142003	0.837	0.000	1.263	1.071
F152000	0.729	0.000	1.283	1.046
F152001	0.698	0.000	1.280	1.043
F152002	0.803	0.000	0.840	1.164
F152003	0.793	0.000	1.629	1.014
F152004	0.849	0.000	1.196	1.077
F152005	0.728	0.000	1.610	0.966
F152006	0.883	0.000	1.206	1.063
F152007	0.864	0.000	1.318	1.062
F162004	0.869	0.000	0.765	1.161
F162005	0.882	0.000	1.108	1.099
F162006	0.928	0.000	0.953	1.132
F162007	0.857	0.000	0.924	1.117
F162008	0.818	0.000	0.854	1.104
F162009	0.676	0.000	0.798	1.045
F182010	0.809	0.000	0.232	1.349
F182011	0.734	0.000	0.670	1.096
F182012	0.732	0.000	0.464	1.175
F182013	0.670	0.000	0.396	1.162

Note.

[a] The sensor information comes from National Oceanic and Atmospheric Administration's (NOAA's) National Centers for Environmental Information.

(2) Year-by-year calibration

Because of the different performance settings of each sensor, even after the self-calibration between images, there is still the problem of discontinuity of remote sensing images of the same year due to the different sensors, and the years of this problem are 1994 and 1997 to 2007, a total of 12 years. The data obtained from different sensors in the same years were calibrated year by year according to equation (2):

$$\mathrm{DN}_{n,i}=\begin{cases}0, & \mathrm{DN}_{n,i}^{a}=0 \text{ and } \mathrm{DN}_{n,i}^{b}=0\\ \dfrac{\mathrm{DN}_{n,i}^{a}+\mathrm{DN}_{n,i}^{b}}{2}, & \text{otherwise}\end{cases} \tag{2}$$

Where $\mathrm{DN}_{n,i}$ represents the calibrated pixel value; n=1997, 2000, ... 2007, representing different years; a and b represent two different sensors in the same year; $\mathrm{DN}_{n,i}^{a}$ represents the pixel value of the i-th cell in the image acquired by sensor a in n-th year.

(3) Continuity calibration

After getting the images of the 12 periods after year-by-year calibration, further continuity calibration needs to be performed, and the calibration conditions set include: If a pixel is detected in an earlier NTL image but disappeared in a later NTL image, it is replaced with values of zero; and the DN value of each lit pixel is corrected to ensure that its DN value in an early NTL image does not exceed its DN value in a later NTL image. The specific calibration model is shown in equation (3):

$$\mathrm{DN}_{(n,i)}=\begin{cases}0, & \mathrm{DN}_{(n+1,i)}=0\\ \mathrm{DN}_{(n-1,i)}, & \mathrm{DN}_{(n+1,i)}>0 \text{ and } \mathrm{DN}_{(n-1,i)}>\mathrm{DN}_{(n,i)}\\ \mathrm{DN}_{(n,i)}, & \text{otherwise}\end{cases} \tag{3}$$

where $\mathrm{DN}_{(n,i)}$ represents the DN value of the i-th cell in the n-th calibration year; $\mathrm{DN}_{(n-1,i)}$ represents the pixel value of the i-th cell in the year before the calibration years; $\mathrm{DN}_{(n+1,i)}$ represents the DN value of the i-th cell in the second year of the calibration years.

After a series of calibration processes, the calibrated nationwide DMSP/OLS NTL dataset from 1992 to 2013 was obtained, and the national images from 2000 and 2010 were selected and extracted as the Baiyangdian basin NTL images by mask, as shown in Figure 2(a) and (b).

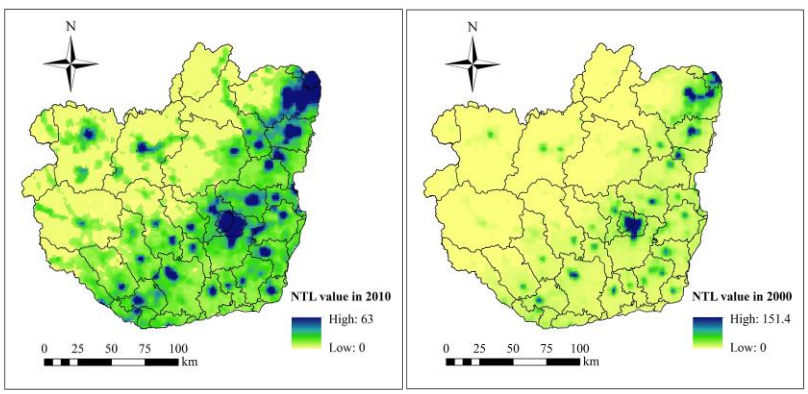

(a) (b)

Figure. 2 Calibrated DMSP/OLS NTL images of Baiyangdian basin in 2000 (a) and 2010 (b).

2.2.2.2 NPP/VIIRS data calibration

(1) Monthly data merged into annual data

Due to the large number of missing data in May to July, 2012 to 2018, these three months were removed when merging into annual data. In addition, to ensure consistency with the DMSP/OLS data, the NPP/VIIRS data was resampled to 1km × 1km resolution and a Gauss-Krueger projection with a central longitude of 117° was performed, and the merged model is shown in equation (4):

$$\mathrm{DN}_{\mathrm{year}}=\frac{\sum_{i=1}^{4}\mathrm{DN}_{\mathrm{month}}+\sum_{i=8}^{12}\mathrm{DN}_{\mathrm{month}}}{9} \tag{4}$$

Where $\mathrm{DN}_{\mathrm{year}}$ represents the DN value of calibrated annual data and $\mathrm{DN}_{\mathrm{month}}$ represents the DN value of monthly data before calibration.

(2) Removing noise

According to the original DMSP/OLS stable NTL data in 2012, a region with DN value equal to 0 was generated, and the NPP/VIIRS data from 2012 to 2018 was extracted based on the generated region to identify its potential threshold of background noise and remove anomalous lights. Weak radiation ($0.3\times10^{-9}\mathrm{W\cdot cm^{-2}\cdot Sr^{-1}}$) was also widely used as a threshold for background noise removal in related studies, [20,21] and in this study, the grids of NPP/VIIRS images with weak NTL radiation ($<0.3\times10^{-9}\mathrm{W\cdot cm^{-2}\cdot Sr^{-1}}$) were removed to further eliminate the influence of background noise.

(3) Consistency calibration with DMSP/OLS images

Since the light saturation condition exists in DMSP/OLS NTL images for all periods, the DN value range of the original DMSP/OLS data was delineated as 0 to 50 as a mask, and the DN values of a total of 96 sets of NPP/VIIRS NTL data from 2012 to 2018 were extracted. After comparative analysis, the power function model with a goodness of fit greater than 0.9 was selected to calibrate the NPP/VIIRS data from 2012 to 2018. The calibration model is shown in equation (5):

$$\mathrm{DN}_{f}=18.34\times\mathrm{DN}_{b}^{0.53}-1.65 \tag{5}$$

Where DN_b represents the DN value before calibration and DN_f represents the DN value after calibration. After processing, the nationwide NTL imagery dataset from 2012 to 2018 can be obtained after fitting with DMSP/OLS, and the image of 2018 was chosen as the study year and extracted as NPP/VIIRS NTL image of Baiyangdian basin by mask, as shown in Figure 3.

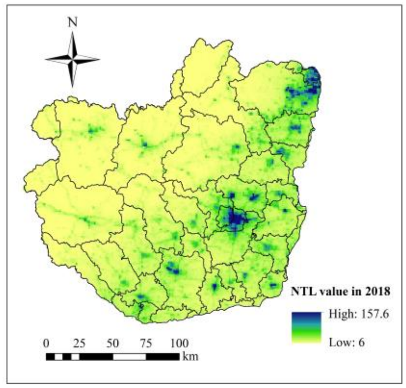

Figure. 3 NPP/VIIRS NTL image of Baiyangdian basin in 2018.

METHODOLOGY

Threshold dichotomy method

In this paper, the reference comparison method based on land use data as auxiliary data was used to determine the lighting thresholds for extracting UCL in each year. Firstly, the potential threshold for extracting UCL in each prefecture-level city was assumed, and the area of urban patches under this threshold was calculated. Let the area of UCL extracted from land use data in Baiyangdian basin be S, the maximum gray value of NTL is DN_{max}, the minimum gray value of NTL is DN_{min}, and the assumed potential threshold value is DN_{thr}. The implementation process of the threshold dichotomy method is shown in Figure. 4. The area of UCL in Baiyangdian basin in 2000, 2010 and 2018 calculated from the land use data are 327km^2, 506km^2 and 585km^2, respectively, from which the optimal NTL thresholds for extracting UCL can be determined as 82, 57 and 58, respectively.

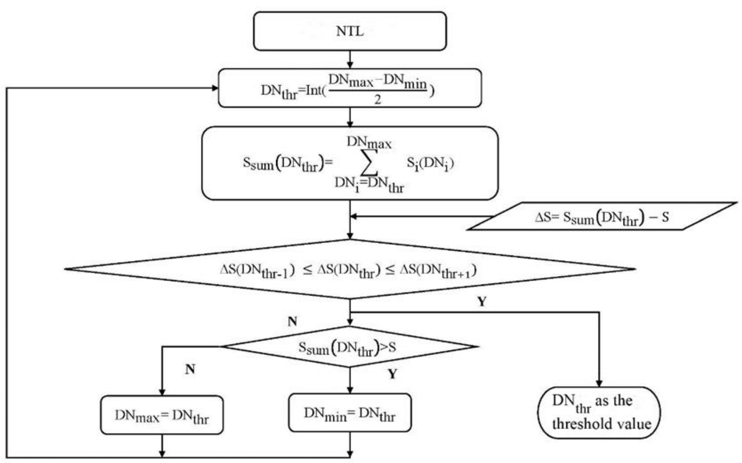

Figure. 4 Flow chart of the threshold dichotomy method to extract UCL.

Landscape metrics analysis

Based on the spatial distribution pattern of UCL extracted by the optimal threshold, this paper used class-level metrics and landscape-level metrics to describe the landscape characteristics of UCL in Baiyangdian basin in 2000, 2010 and 2018. The selected metrics include area metrics (Total Landscape Area, TA; Largest Patch Index, LPI), density size and difference metrics (Patch Density, PD), edge metrics (Edge Density, ED; Perimeter-Area Fractal Dimension, PAFRAC), shape metrics (Landscape Shape Index, LSI), dispersion metrics (Contagion Index, CONTAG), and diversity metrics (Shannon's Diversity Index, SHDI). Among them, the unit of TA is ha; LPI indicates the proportion of the largest patch to the landscape area; the unit of PD is patch number /100 ha; the unit of ED is m/ha; PAFRAC indicates the complexity of traits at different spatial scales, and the range of values is 1 to 2, the closer to 1 means the simpler the shape of patches, the closer to 2 means the more complex the shape of patches and the less the degree of human interference; CONTAG can describe the extension trend of the patch types in the landscape, a large value means the dominant patch types in the landscape form a good connection, on the contrary, the landscape shows the distribution of multiple elements, and the degree of fragmentation is high; as for SHDI, in the landscape system, the richer the land use, the larger the value of SHDI, while the SHDI value of 0 means that the whole landscape is composed of only one patch.

Gravity model

The existing research on the change law of the center of gravity of UCL is only based on the general boundary of UCL, ignoring the information of non-UCL, which leads to the problem that the calculation of the center of gravity of UCL is not objective and accurate. Zhao et al. (2015) applied the NTL intensity to the study of urban expansion and constructed a new urban gravity model.[22] Accordingly,

$$D_{ij} = \frac{D_{min} \times D_{max}}{2} \tag{6}$$

$$X_C = \frac{\sum_{j=1}^{n} (x_{ij} D_{ij})}{\sum_{j=1}^{n} C_{ij}} \tag{7}$$

where D_{min} represents the minimum value of the NTL gray value of the *j*-th kernel density area in the *i*-th year; D_{max} represents the maximum value of the NTL gray value of the *j*-th kernel density area in the *i*-th year; D_{ij} represents the average value of the NTL gray value of the *j*-th kernel density area in the *i*-th year; X_C and Y_C respectively represent the latitude and longitude coordinate values of the center of gravity in the *i*-th year; x_{ij} and y_{ij} respectively represent the latitude and longitude coordinate values of the center of gravity of the *j*-th kernel density area; *n* represents the number of kernel density areas.

RESULTS AND DISCUSSION

Extraction results of UCL

we firstly analyzed the NTL data of Baiyangdian basin in 2000, 2010, and 2018 for kernel density, and distinguished the kernel density into nine grades from 1 to 9. The higher the grade, the greater the NTL brightness value and the greater the intensity of urban activity. Secondly, the center of gravity coordinates of the nine homogeneous spaces were calculated. Finally, according to the NTL value, the nine center of gravity coordinates were given corresponding weights, and the final urban center of gravity coordinates were calculated. The specific weighting process and the formula for calculating the urban center of gravity coordinates in *i*-th year are shown in equation (6-8):

$$Y_C = \frac{\sum_{j=1}^{n} (y_{ij} D_{ij})}{\sum_{j=1}^{n} C_{ij}} \tag{8}$$

The extraction information and distribution of UCL in Baiyangdian basin are shown in Table 2 and Figure. 5. As can be seen from Table 2, the area of UCL in Baiyangdian basin was 304 km^2 in 2000, 466 km^2 in 2010 and 527 km^2 in 2018. During the study period, the area of UCL in Baiyangdian basin has been increasing year by year, showing the characteristics of multiple centers and expanding in a plane shape, initially showing the continuous spread of urban boundary. After further quantitative analysis of the distribution pattern of UCL, it is clear that although the area of UCL is increasing every year, its expansion rate is decreasing with the increase of time, and it is 16.2% in the first ten years of the study period, while it decreases to 6.1% in the second ten years. Overall, such a changing trend is favorable to the intensive and efficient use of urban space.

Table 2 Statistics of NTL values in Baiyangdian basin

Year	Total DN value	DN_{max}	DN_{thr}	UCL area/km^2
2000	34507	151	82	304
2010	28292	63	57	466
2018	41153	157	58	527

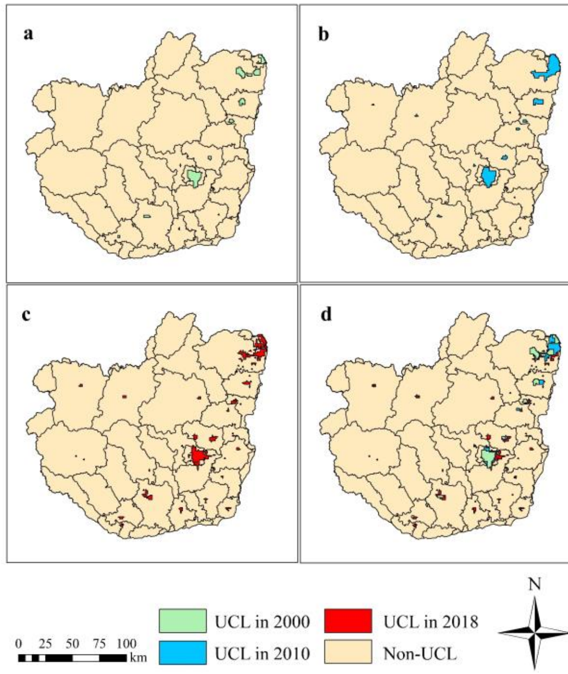

Figure. 5 Distribution of UCL in Baiyangdian basin from 2000 to 2018 (a, b, c) and superimposed map (d).

Landscape pattern analysis

According to the NTL map of the UCL in Baiyangdian basin extracted by the threshold method and the landscape metrics analysis using Fragstats 4.2 software, the results are shown in Figure. 6. In terms of NP, the value gradually decreased from 222 to 137 from 2000 to 2010, and the fragmentation decreased, while the value jumped to 425 in 2018, which indicates that on the whole, the UCL in Baiyangdian basin does not tend to be centralized development, and similarly the CONTAG also reached the lowest value of 17.24 in 2010, which indicates that the degree of fragmentation is low and the concentration is good in Baiyangdian basin in 2010, but it rose to 23.07 in 2018, and the phenomenon of urban sprawl appeared again; TA has increased from 304 km^2 to 527 km^2 during the study period, but its growth rate slowed down; PD showed a trend of sharp decline and then sharp increase, reaching the lowest value in 2010 with a density value of about 0.27/ha, and finally was 0.74/ha in 2018; SHDI showed similar evolutionary characteristics, reaching a minimum value of 1.86 in 2010 and rising steeply to 3.88 in 2018, indicating that the land use types in the Baiyangdian basin ushered in a second increase after experiencing a pattern of yearly decrease; the change trend of LPI was rising at first and then falling, with the highest proportion of 15.02% in 2010; ED was decreasing in general, which also indicates the rapid expansion of UCL in Baiyangdian basin; LSI reached the lowest in 2010 and the highest in 2018, with 7.84 and 14.38 respectively; PAFRAC increased slightly between 2000 and 2010, but showed a decreasing characteristic overall, which from the side illustrates that the development of cities first experienced a period of concentrated development, and then evolved into spreading development.

Shift pattern of center of gravity of UCL

At present, the existing research shows that the change of China's city center of gravity shows four types of distribution characteristics, which are basic fixed type, one-way migration type, deflection migration type and round-trip migration type. The basic fixed type means that the center of gravity of a city remains basically unchanged at its original position, representing cities such as Hohhot and Urumqi; the one-way migration type means that the center of gravity of a city changes in a single direction, representing cities such as Guangzhou, Nanjing and Shanghai; the deflection migration type means that the center of gravity of a city moves in one direction and then deflects in another direction, representing cities such as Tianjin, Foshan and Lanzhou; the round-trip migration type means that the center of gravity of a city is distributed in a round-trip manner, moving in a certain direction and then changing in the opposite direction, and finally turning back to the initial direction, representing city like Hefei.

From Figure. 7, it is obvious that the center of gravity of cities in Baiyangdian basin is of the deflection migration type, with the longitude and latitude of the center of gravity changing from (115.72°E, 39.24°N) to (115.66°E, 39.21°N) from 2000 to 2010, and to (115.68°E, 39.15°N) in 2018. Geographically, influenced by the strong NTL intensity in the main urban area of Baoding, Fangshan District and Fengtai District of Beijing, the center of gravity of the basin is located in Dingxing County of Baoding, and its longitude and latitude coordinates first move along the southwest direction, and then change toward the southeast.

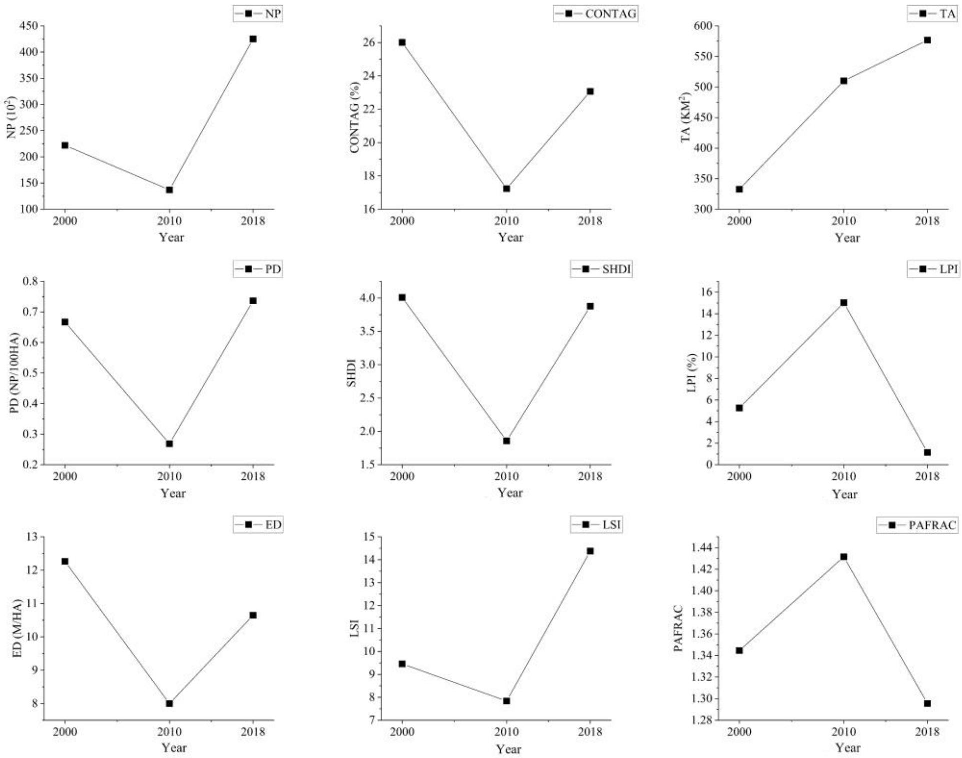

Figure. 6 Landscape metrics of UCL patches in Baiyangdian basin.

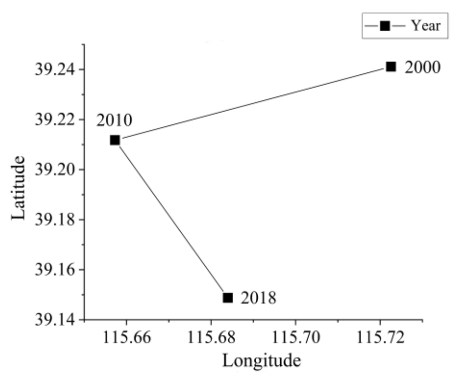

Figure. 7 Migration track of the center of gravity of UCL in Baiyangdian basin.

Comparison with other related methods

In order to reflect the higher extraction accuracy of our method more intuitively, we used the unfitted and uncalibrated NPP/VIIRS data (method 1) and the reference comparison method based on long time series NTL data and traditional statistical data (method 2) respectively to extract the UCL in Baiyangdian basin in 2018. The evaluation indexes involved include recall, precision and F1 score, in which F1 score takes into account both recall and precision, which is the harmonic mean of both. The extraction results of each method are shown in Table 3. It can be seen that no matter which evaluation index, the method proposed in our paper based on long time series NTL data and land use data for extracting the UCL is obviously superior to the other two methods.

Table 3 Accuracy assessment on the extraction results

	Method 1	Method 2	Our method
Recall	0.74	0.79	0.86
Precision	0.68	0.72	0.83
F1 score	0.71	0.75	0.84

Further discussion

Although this paper extracted UCL by a more scientific long time series NTL fitting method, making the research results more accurate, there are still shortcomings. For example, though the combination of NTL data and land use data achieves the spatio-temporal characteristics of UCL in the long time series, its spatial resolution is still 1km×1km, which cannot achieve higher resolution boundary identification, while in future research, the long time series extraction of higher resolution can be carried out, which is conducive to a more refined quantitative study of UCL. What’s more, there is no specific analysis of the driving factors in the expansion of UCL, but a detailed exposition of its evolution law, which needs further consideration and discussion.

CONCLUSION

The spatial resolution of the NTL dataset established in this paper was 1km×1km, and the influences of noise and saturation of NTL were eliminated, and the problem of discontinuity of DN values between different sensors was also calibrated, besides, the NPP/VIIRS data fitting calibration based on the DMSP/OLS data was carried out, and the land use data and statistical data were combined for auxiliary validation, which finally formed the long time series NTL dataset from 1992 to 2018, which made it possible to analyze the spatio-temporal patterns and laws of UCL changes over long time periods. Besides, by comparing with other methods about extracting UCL, our method has obvious advantages in recall rate, precision rate and F1 score.

After extracting and characterizing the UCL in Baiyangdian basin, we found that the urban expansion in the basin showed a polycentric and faceted expansion, for example, Fengtai District and Fangshan District in Beijing, Jingxiu District and Lianchi District in Baoding all had large UCL distributed and spread in all directions, and the problem of urban expansion became more and more prominent. From the landscape metrics, the basin showed a concentrated development trend from 2000 to 2010, but tended to be dispersed from 2010 to 2018, which also shows that the urban land in the basin is expanding and spreading. From the overall migration track of the center of gravity of the basin, the center of gravity was located in Dingxing County, between main urban area of Baoding and Beijing, showing the deflection migration type, that was, the migration occurred first in the southwest direction and then in the southeast direction during 2010 to 2018.

It is alsofound that reasonable modern tobacco agricultural planning will have a certain impact on the distribution of UCL. With the gradual development of tobacco agriculture, its impact on UCL is becoming more and more obvious. The area of UCL in areas with larger tobacco agricultural land is smaller and distributed more dispersedly while the area of UCL in the area with smaller tobacco agricultural land is larger and the distribution is more concentrated. Tobacco agriculture planning also has a great influence on the distribution center of UCL, that is, it will guide the center of gravity to move towards the places where tobacco agricultural land occupies a relatively small proportion. To sum up, our research can provide method and experience reference for regional scientific and rational modern tobacco agricultural planning and land use.

Author Declaration

This research is not funded by any organization related to tobacco production.

Acknowledgements

The authors acknowledge the National Social Science Fund of China (Grant: 17BTJ029).

References

1. Frechtling JA, Dunderdale T, Price S, et al. Establishing a Research Base to Inform Tobacco Regulation: Overview. Tob Regul Sci. 2021;7(2):144-154. doi:10.18001/TRS.7.2.6
2. Levy DT, Chaloupka F, Lindblom EN, et al. The US Cigarette Industry: An Economic and Marketing Perspective. TobRegulSci.2019;5(2):156-168. doi:10.18001/TRS.5.2.7
3. Xu H, Du L. Fast extraction of built-up land information from remote sensing imagery. Journal of Geo-information Science.2010;12(4):574-579.doi: CNKI:SUN:DQXX.0.2010-04-020
4. Croft T A. Nighttime images of the earth from space. Sci Am.1978;239(1):86-98.doi: 10.1038/scientificamerican0778-86
5. Song G,Wang Y. Spatial and temporal distribution of land use pattern change in Songnen high plain. Transactions of the Chinese Society of Agricultural Engineering.2016;32(18):225-233.doi: 10.11975/j.issn.1002-6819.2016.18.031
6. Su L, Guo Y, Wu Y, et al. Dynamic change of land use types in Linzhi prefecture of Tibet based on RS and GIS. Journal of China Agricultural University. 2019;24(10):170-178.doi: 10.11841/j.issn.1007-4333.2019.10.19
7. Zhou Y, Smith SJ, Elvidge CD, et al. A cluster-based method to map urban area from DMSP/OLS nightlights. Remote Sens Environ. 2014;147(18):173-185.doi: 10.1016/j.rse.2014.03.004
8. Huang L, Yang B, Zhu Q. Expansion research on the build up area in Nanjing City based on DMSP/OLS data. Geospatial Information.2018;16(1):94-97.doi: 10.3969/j.issn.1672-4623.2018.01.028
9. Ma T, Zhou Y, Zhou C, et al. Night-time light derived estimation of spatio-temporal characteristics of urbanization dynamics using DMSP/OLS satellite data. Remote Sens Environ. 2015;158: 453-464.doi: 10.1016/j.rse.2014.11.022
10. Zhou Y, Smith SJ, Zhao K. A global map of urban extent from nightlights. Environ Res Lett.2015;10(5):1-11.doi: 10.1088/1748-9326/10/5/054011
11. Xie Y, Weng Q. Updating urban extents with nighttime light imagery by using an object-based thresholding method.

Remote Sens Environ.2016;187:1-13.doi: 10.1016/j.rse.2016.10.002
12. Shi K, Huang C, Yu B, et al. Evaluation of NPP/VIIRS night-time light composite data for extracting built-upurban areas. Remote SensLett.2014;5(4):358-366.doi: 10.1080/2150704X.2014.905728
13. Dong C, Cao Y, Tan Y. Urban expansion and vegetation changes in Hangzhou Bay area using night-light data. Chinese Journal of Applied Ecology.2017;28(1):231-238.doi: 10.13287/j.1001-9332.201701.022
14. Liu Z, He C, Zhang Q, et al. Extracting the dynamics of urban expansion in China using DMSP-OLS nighttime light data from 1992 to 2008. Landsc Urban Plan.2012;106(1):62-72.doi: 10.1016/j.landurbplan.2012.02.013
15. Liu Z, Zhang Q, Yue D, et al. Extraction of urban built-up areas based on Sentinel-2A and NPP-VIIRS nighttime light data. Remote Sensing for Land & Resources.2019;31(04):227-234.doi: 10.6046 /gtzyyg.2019.04.29
16. Li J, Pan J. Spatial expansion of cities at county-level or above in Gansu Province from 1992 to 2012 based on DMSP nighttime light images. Journal of Glaciology and Geocryology.2016;38(03):829-835.doi: 10.7522/j.issn.1000-0240.2016.0093
17. Li J, Gong J, Yang J, et al. Urban spatial pattern evolution of Wuhan City based on nighttime light. Remote Sensing Information.2017;32(03):133-141.doi: 10.3969/j.issn.1000-3177.2017.03.022
18. Yuan R, Song X. Boundary Data of the Baiyangdian Lake Basin. Digital Journal of Global Change Data Repository. 2020. doi:10.3974/geodb.2020.05.18.V1
19. Dong H, Li R, Li J, et al. Study on urban spatiotemporal expansion pattern of three first-class urban agglomerations in China derived from integrated DMSP-OLS and NPP-VIIRS nighttime light data. Journal of Geo-information Science.2020;22(05):1161-1174.doi: 10.12082/dqxxkx.2020.190711
20. Chen L, Ren C, Zhang B, et al. Quantifying urban land sprawl and its driving forces in northeast China from 1990 to 2015. Sustainability.2018;10(1):1-18.doi:10.3390/su10010188
21. Ma T, Zhou C, Pei T, et al. Responses of Suomi-NPP VIIRS-derived nighttime lights to socioeconomic activity in China's cities. Remote SensLett.2014;5(2):165-174.doi: 10.1080/2150704X.2014.890758
22. Zhao M, Cheng W. Overview of researches based on urban expansion via DMSP/OLS night-time light data. Geomatics & Spatial Information Technology.2015;38(03):64-68.doi: CNKI:SUN:DBCH.0.2015-03-021